ACSNANO
www.acsnano.org
ARTICLE

Superconducting Calcium-Intercalated Bilayer Graphene

Satoru Ichinokura,*[,†] Katsuaki Sugawara,[‡] Akari Takayama,[†] Takashi Takahashi,[‡,§] and Shuji Hasegawa[†]

[†]Department of Physics, University of Tokyo, Tokyo 113-0033, Japan
[‡]WPI Research Center, Advanced Institute for Materials Research, Tohoku University, Sendai 980-8577, Japan
[§]Department of Physics, Tohoku University, Sendai 980-8578, Japan

ABSTRACT: **We report the direct evidence for superconductivity in Ca-intercalated bilayer graphene C_6CaC_6, which is regarded as the thinnest limit of Ca-intercalated graphite. We performed the electrical transport measurements with the *in situ* 4-point-probe method in ultrahigh vacuum under zero- or nonzero-magnetic field for pristine bilayer graphene, Li-intercalated bilayer graphene (C_6LiC_6) and C_6CaC_6 fabricated on SiC substrate. We observed that the zero-resistance state occurs in C_6CaC_6 with the onset temperature (T_c^{onset}) of 4 K, while the T_c^{onset} is gradually decreased upon applying the magnetic field. This directly proves the superconductivity origin of the zero resistance in C_6CaC_6. On the other hand, both pristine bilayer graphene and C_6LiC_6 exhibit nonsuperconducting behavior, suggesting the importance of intercalated atoms and its species to drive the superconductivity.**

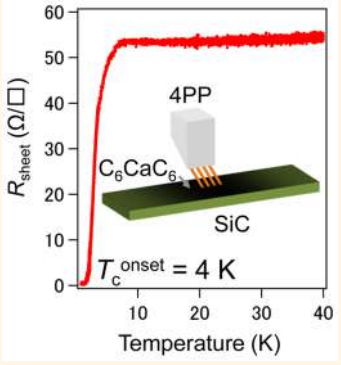

KEYWORDS: *graphene, superconductivity, electrical transport, carbon, semiconductor surface, graphite-intercalation-compound, ultrahigh vacuum*

Atomic layer superconductors (ALSCs), where only one or a few atomic layers at the surface or interface becomes superconducting,[1−5] have attracted considerable attentions owing to their strong two-dimensionality. ALSCs composed of bulk-superconducting metallic elements such as In and Pb are usually fabricated on a semiconductor substrate,[1−4] and generally show the superconducting-transition temperature (T_c) lower than that of bulk[1−3] due to the strong interference from the substrate. On the other hand, it is expected that the interference from the substrate is considerably reduced in the case of two-dimensional (2D) materials such as transition-metal dichalcogenides and graphite, which show the superconductivity by itself or when it is doped with excess carriers.[6,7] To widen the possibility for architecting the electronic devices based on ALSCs, intensive studies have been in progress to fabricate self-standing atomically thin 2D superconductors.

Graphene is a one-atomic-layer-honeycomb-network of carbon atoms and inherently has a strong 2D nature and various novel properties such as the massless electrons,[8] the high carrier mobility,[9] and the remarkable mechanical strength and flexibility.[10] Several methods, such as mechanical exfoliation[11] and epitaxial growth on various substrates,[11,12] have been employed to obtain a high-quality graphene film with a large working area, especially for application to electronic devices. Superconducting graphene has been a target of intensive studies since the discovery of graphene,[13] because it realizes an intrinsic self-standing 2D ALSC.[14,15] Many intensive efforts have been made to fabricate superconducting graphene by doping metals like in bulk graphite intercalation compounds (GICs).[16−19] Since metal-doped graphene is unstable in air because of the high reactivity of intercalated metals, an *in situ* measurement in ultrahigh vacuum (UHV) is required to observe the possible superconductivity. A recent *in situ* angle-resolved photoemission spectroscopy (ARPES) reported the opening of an energy gap at the Fermi level (E_F) at low temperatures in Li-decorated monolayer graphene,[16] suggesting the occurrence of superconductivity in doped graphene. However, it is not clear whether the gap-like feature observed by ARPES is due to the superconductivity or other origins such as charge-density-waves. Thus, it is urgent to clarify/confirm the origin of the gap-like feature by other more direct macroscopic measurements such as the zero resistance at low temperatures.

In this paper, we report an *in situ* resistivity measurement in UHV on Ca-intercalated bilayer graphene (C_6CaC_6). It is known that Ca-intercalated graphite (C_6Ca) has the highest T_c of 11.5 K among all GICs,[20−24] and it has been theoretically proposed that C_6CaC_6 becomes superconductive with a relatively high transition temperature.[14,15] In fact, previous transport and magnetic measurements[25,26] reported that Ca-doped multilayer graphene shows the superconductivity with T_c

Received: December 14, 2015
Accepted: January 27, 2016

DOI: 10.1021/acsnano.5b07848
ACS Nano XXXX, XXX, XXX−XXX

(6−7 K) slightly lower than that of bulk C_6Ca. However, these previous measurements were done *ex situ* with exposing the sample to air, although, as described above, metal-doped graphene is very reactive in air and the possibility of deterioration of sample is not excluded. Further, the number of graphene layers in these "multilayer" graphene is not necessarily clear. To firmly establish the superconductivity in Ca-doped graphene, it is essential to perform an *in situ* experiment under UHV with a well-characterized graphene sample. In the present study, we clearly observed the zero resistance in Ca-intercalated bilayer graphene (BLG), which is regarded as the thinnest limit of bulk Ca-intercalated graphite, by the *in situ* four-terminal method[27] combined with the UHV scanning tunneling microscopy (STM). We have confirmed that the superconductivity is the origin of the observed zero-resistance from the measurements under magnetic field.

RESULTS AND DISCUSSION

To fabricate intercalated BLG (Figure 1a), we at first prepared a pristine BLG sheet on a n-type Si rich 6*H*-SiC(0001) single

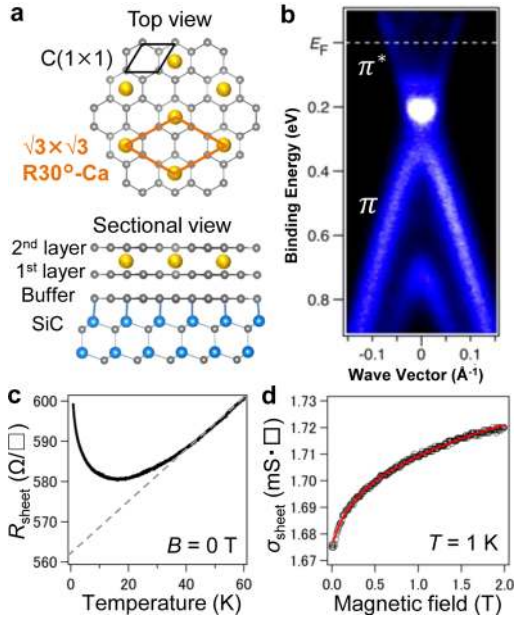

Figure 1. Characterization of pristine bilayer graphene. (a) Schematic view of crystal structure of C_6CaC_6 on SiC. (b) Band dispersions at K point of pristine bilayer graphene. (c and d) Transport characteristics of pristine bilayer graphene. (c) Temperature dependence of sheet resistance under zero magnetic field. Dashed line shows extrapolation toward 0 K. (d) Magnetic field dependence of sheet conductance at 1 K. Black circles denote experimental data and red line is the numerical fitting by Hikami−Larkin−Nagaoka equation for bilayer graphene.[31]

crystal by heating it up to 1550 °C in an argon atmosphere.[28] By controlling the heating temperature and the duration time, we selectively synthesized BLG, excluding mono- and trilayer graphene. Figure 1b shows the band dispersions around the K point in the Brillouin zone for our BLG sample, obtained by *in situ* ARPES measurements. One can clearly see *two* π bands in the vicinity of E_F, directly proving that the sample is *bilayer* graphene, because mono- and trilayer graphene should show one and three π bands,[29] respectively. We also notice that a part of the π^* band is located below E_F due to the charge transfer from the buffer layer and SiC substrate.[28,29]

Figure 1c shows the temperature-dependent transport characteristics of BLG below 60 K, where the conductivity in SiC substrate is negligible. The sheet resistance (R_{sheet}) of BLG shows a metallic behavior above 20 K, but turns into the insulating one at low temperatures. This is usually observed in the transport characteristics of epitaxial graphene on SiC and ascribed to the electron−electron scattering and the weak localization effect, suggesting the strong two-dimensional nature of BLG.[30] The residual resistance at 0 K is roughly estimated to be 560 Ω. The effect of weak localization is seen in the magnetotransport measurement at 1 K (Figure 1d), and the experimental result is well fitted by Hikami−Larkin−Nagaoka equation.[31] From the fitting, we have estimated the relaxation length of intervalley- and intravalley-scattering at 54 ± 8 and 36 ± 1 nm, respectively. This result is consistent with the report for monolayer graphene on SiC, where the momentum relaxation length is dominated by the intravalley-scattering due to the donors' potential distributed randomly on SiC surface.[30]

After a short exposure to air, the grown BLG was transferred into another vacuum chamber where the transport measurements and the check of surface by RHEED (reflection-high-energy electron diffraction) were performed. After the sample was heated at 400 °C for several hours in the chamber, we observed the RHEED pattern typical of clean BLG on SiC (Figure 2a). Both Si(1 × 1) spots from the substrate and C(1 ×

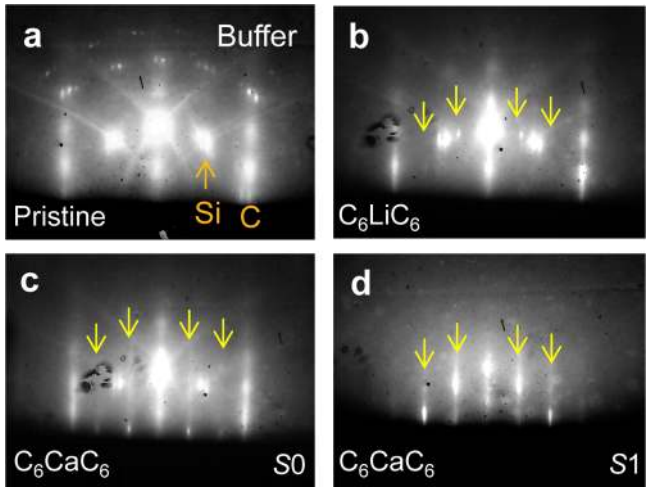

Figure 2. Evolution of the RHEED patterns during intercalation process. (a) Thermally cleaned pristine bilayer graphene. (b) C_6LiC_6. (c and d) C_6CaC_6 (c) after the first Li−Ca replacing treatment and (d) after several cycles of the replacing treatments. Yellow allows indicate $\sqrt{3} \times \sqrt{3}R30°$ spots and streaks.

1) spots from graphene are clearly seen. Spots from the buffer layer with the $6\sqrt{3} \times 6\sqrt{3}R30°$ periodicity are also visible. When we evaporated Li atoms onto this BLG sheet, several sharp $\sqrt{3} \times \sqrt{3}R30°$ spots emerged in the RHEED pattern (yellow arrows in Figure 2b), indicating that Li atoms are regularly intercalated between two adjacent graphene layers.[32] After confirming the growth of Li-intercalated BLG (C_6LiC_6), we then deposited Ca atoms on this C_6LiC_6 sheet to replace Li with Ca atoms. During the Ca deposition, we kept the substrate at 150 °C, slightly above the Li desorption temperature of 145 °C. The Ca deposition transformed the $\sqrt{3} \times \sqrt{3}R30°$ spots into streaks (Figure 2c), suggesting that intercalated Li atoms are replaced by Ca atoms.[17] However, not all the area of sample

DOI: 10.1021/acsnano.5b07848
ACS Nano XXXX, XXX, XXX−XXX

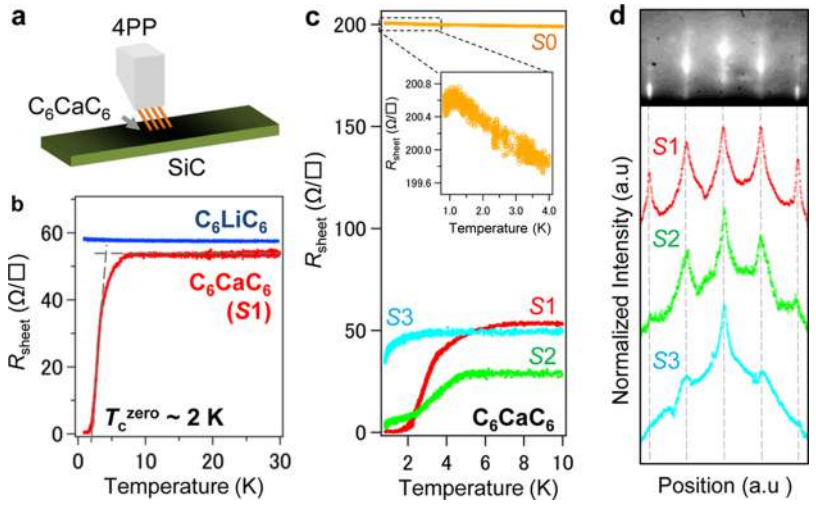

Figure 3. Temperature dependence of transport characteristics for Li- and Ca-intercalated bilayer graphene under zero magnetic field. (a) Schematic picture of 4-point-probe measurement setup. (b) Comparison of temperature dependence of sheet resistance R_{sheet} between C_6LiC_6 (blue) and C_6CaC_6 (Sample *S*1, red). C_6CaC_6 exhibits superconducting transition with T_c^{onset} = 4 K and T_c^{zero} = 2 K. (c) Comparison of temperature dependence of R_{sheet} among samples *S*0−*S*3. Inset shows R_{sheet} of sample *S*0 from 0.8−4.0 K. (d) Line profiles of RHEED patterns for samples *S*1−*S*3. The intensity is normalized with the peak height of the central (1 × 1) streak. The upper column shows the RHEED picture of sample *S*1.

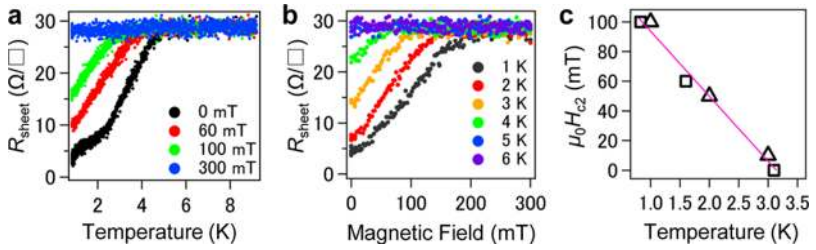

Figure 4. Magnetoresistance of Ca-intercalated bilayer graphene. (a) R_{sheet} of C_6CaC_6 (sample *S*2) as a function of temperature under different magnetic fields. (b) Same as (a) as a function of magnetic field for different temperatures. The magnetic field was applied perpendicular to the sample surface. (c) Temperature dependence of the upper critical field $\mu_0 H_{c2}$ obtained from (a) (squares) and (b) (triangles). The value of $\mu_0 H_{c2}$ was defined as the magnetic field where R_{sheet} drops to a half of normal-state resistance in (a) and (b). Solid line shows the fit with the Ginzburg−Landau theory.[34]

was converted into C_6CaC_6 at this early stage, because repeated cycles of Li and Ca deposition together with annealing made the $\sqrt{3} \times \sqrt{3}R30°$ streaks brighter and brighter. We call the sample at this early stage sample *S*0. After several cycles of Ca-deposition and annealing, we finally obtained the very sharp $\sqrt{3} \times \sqrt{3}R30°$ streaks in the RHEED pattern (Figure 2d), indicative of formation of well-ordered C_6CaC_6. We call this sample *S*1.

After fabrication of the sample as described above, we then performed the *in situ* electrical transport measurement in the same vacuum chamber with the 4-point-probe (4PP) method.[27] As shown in Figure 3a, the 4PP chip was contacted on the sample, and then cooled down to 0.8 K together with the sample. The results of temperature-dependent transport measurements on C_6LiC_6 and C_6CaC_6 (sample *S*1) are compared in Figure 3b. In contrast to the pristine BLG (Figure 1c), the R_{sheet} of intercalated BLG behaves as metallic, and their resistance is as low as *ca.* 10% of that of pristine BLG. This is because of the increase of the Fermi-surface volume by the carrier doping from Li or Ca atoms and the resultant folding of Brillouin zone due to the induced $\sqrt{3} \times \sqrt{3}R30°$ superstructure.[17] Importantly, the transition of R_{sheet} to zero-resistance is clearly seen at around 2 K in C_6CaC_6, which is the direct evidence for macroscopically coherent superconductivity with T_c^{zero} = 2 K. It is also noteworthy that C_6LiC_6 shows no sign of superconductivity down to 0.8 K, and instead exhibits a weak localization behavior as evident from a slight upturn in resistance at low temperatures. While the R_{sheet} of C_6CaC_6 shows a sharp drop at around 4 K (T_c^{onset} = 4 K), it starts to decrease even above 4 K as seen in Figure 3b. This may be due to the superconducting fluctuation inherent to low-dimensional superconductors.[33]

Figure 3c shows the sample-dependent R_{sheet} as a function of temperature. Three samples (*S*1−*S*3) prepared with the same method as described above reproducibly exhibited superconducting transition. The difference in quality among samples *S*1−*S*3 is seen in the line profile of RHEED pattern (Figure 3d). The central peak is due to the 1 × 1 structure, while the side peaks are from the $\sqrt{3} \times \sqrt{3}R30°$ superstructure originating from the intercalated Ca sheet. Figure 3c,d shows that the R_{sheet} at 0.8 K approaches the zero-resistance when the $\sqrt{3} \times \sqrt{3}R30°$ spot becomes stronger. The fact that *S*1 with the brightest $\sqrt{3} \times \sqrt{3}R30°$ spot shows a full drop to zero-resistance at 2 K suggests that the ordering in the Ca layer is important to realize the superconductivity. This is confirmed by the experimental fact that the R_{sheet} of sample *S*0 (early stage sample) shows only a tiny drop near the lowest temperature.

DOI: 10.1021/acsnano.5b07848
ACS Nano XXXX, XXX, XXX−XXX

To obtain further evidence for the superconductivity, we conducted magnetoresistance measurements on C_6CaC_6 (sample *S2*), under the magnetic field perpendicular to the sample surface. Panels a and b in Figures 4 show R_{sheet} as a function of temperature and magnetic field, respectively. As seen in Figure 4a, the T_c^{onset} is gradually shifted toward lower temperature as the magnetic field is increased. A similar behavior of T_c^{onset} is also seen in Figure 4b. To see the temperature-dependence of the upper critical field ($\mu_0 H_{c2}$), we plot in Figure 4c the magnitude of magnetic field at which the R_{sheet} is a half of the normal-state-resistance as a function of temperature. The $\mu_0 H_{c2}$ at 1 K is 100 mT, which is four times larger than that reported in Ca-intercalated 50-layers graphene[25] and is almost the same as that of bulk C_6Ca.[20,21] We find that the obtained $\mu_0 H_{c2}$ values are well aligned linearly, which suggests that the experimental results can be analyzed in the framework of the Ginzburg−Landau (GL) theory.[34] Numerical fittings with the GL theory show that the in-plane GL coherence length at zero Kelvin $\xi(0)$ is 49 ± 1 nm. This value is comparable to the momentum relaxation length of pristine BLG, obtained from the analysis of weak localization in Figure 1d. This indicates that the superconducting coherence length in C_6CaC_6 is limited by scattering at random potential on the SiC surface. However, the $\xi(0)$ in C_6CaC_6 is slightly larger than that of bulk C_6Ca (29−36 nm),[20,21] probably owing to the high career mobility in graphene. This shows a striking contrast to the case of usual ALSCs such as In on Si(111), where the $\xi(0)$ is ∼25 nm [ref 3] and much shorter than that of bulk (250−440 nm).[35] This suggests the strong 2D nature of superconductivity in C_6CaC_6.

Next we comment on recent progresses in superconducting graphene in relation to the present experimental results. Recently, the superconductivity in Li-decorated *monolayer* graphene[16] was reported, showing a marked contrast to the present observation of absence of superconductivity in Li-intercalated *bilayer* graphene. This, in return, provides an important experimental clue to elucidate the origin and mechanism of superconductivity in graphene and graphite. Ludbrook *et al.*[16] observed a free-electron-like metallic band at the Γ point in their superconducting Li-decorated monolayer graphene, in good agreement with the calculation which has predicted a strong electron−phonon coupling in metal-decorated monolayer graphene.[36] On the other hand, it has been also theoretically predicted that the free-electron-like band is located above E_F in Li-intercalated *bilayer* graphene,[37] as revealed by ARPES experiments.[17,32] These theoretical and experimental studies indicate that the free-electron-like metallic band is essential to realize the superconductivity in metal-doped graphene and the electron−phonon coupling is enhanced in monolayer graphene.[36] It is noted here that the free-electron-like metallic band is also seen in Ca-intercalated bilayer graphene.[17] It is also important to comment on the experimental fact that the T_c (2 K) of Ca-intercalated bilayer graphene (C_6CaC_6) is lower than that of Ca-doped multilayer graphene (6−7 K)[25,26] and Ca-intercalated graphite (C_6Ca, T_c = 11.5 K).[20−24] The difference in T_c among these compounds may be due to the difference in the amount of doped electrons per a single graphene sheet. In bulk GICs, the first-stage compound such as C_8K, which consists of a single K layer per a single carbon (graphene) layer, shows the superconductivity, while the second-stage compound such as $C_{16}K$ composed of a single K layer per two graphene layers does not show the superconductivity. The absence of superconductivity in the second-stage compound is ascribed to the insufficient electron doping from the K layer because of the reduced population of K layers in the compound. Ca-intercalated bilayer graphene (C_6CaC_6) corresponds to a single layer of structural unit of the second-stage Ca-intercalated graphite ($C_{12}Ca$), while intercalated multilayer graphene is much closer to the first stage compound (C_6Ca). It is inferred that the situation of charge balance in intercalated *multilayer* graphene is closer to that of bulk C_6Ca than that of *bilayer* graphene, resulting in the difference in T_c between Ca-doped bilayer and multilayer graphene.

CONCLUSIONS

In conclusion, we performed the *in situ* electrical transport measurements on Ca-intercalated bilayer graphene (C_6CaC_6). We have observed that the resistance steeply drops at 4 K and reaches zero at 2 K under zero magnetic field, demonstrating the emergence of superconductivity with T_c^{onset} = 4 K and T_c^{zero} = 2 K. The measurements under magnetic field have confirmed that the observed zero resistance is of superconductivity origin.

MATERIALS AND METHODS

Bilayer graphene was prepared by heating a *n*-type Si-rich *6H*-SiC(0001) single crystal at 1550 °C with resistive heating under 0.1 MPa Ar gas.[28] To confirm the number of graphene layers in the sample, we performed ARPES measurements using a VG-Scienta SES2002 spectrometer with a high-flux helium discharge lamp. The atomic force microscopy (AFM) measurements showed the typical terrace size of ∼5 μm. Deposition of Li was carried out using a Li dispenser (SAES Getters), while Ca was deposited with a Knudsen-cell under UHV of 5 × 10^{-10} Torr. RHEED measurements were performed with the primary electron energy of 14 keV. The electrical transport measurements were done with Unisoku USM-1300S,[27] where a 4PP consisting of four copper wires with 100 μm diameter was attached to the STM head. The sheet resistance R_{sheet} was obtained by the 4PP dc current−voltage measurement, by using the dual configuration method to avoid data scattering due to the error of probe contact point.[27] To avoid Joule heating during the measurement, the applied current was controlled to be less than 6 μA. The minimum resistance we could measure was 5 Ω. All the 4PP measurements were performed in a vacuum better than 3 × 10^{-10} Torr. No degradation of the sample surface was observed during the measurements.

AUTHOR INFORMATION

Corresponding Author

*E-mail: ichinokura@surface.phys.s.u-tokyo.ac.jp.

Notes

The authors declare no competing financial interest.

ACKNOWLEDGMENTS

We thank R. Akiyama and Y. Endo at University of Tokyo, and K. Suzuki and T. Sato at Tohoku University for their useful discussions. This work was supported by the JSPS (KAKENHI 15H02105, 25246025, 22246006) and the MEXT (Grant-in-Aid for Scientific Research on Innovative Areas "Science of Atomic Layers" 25107003 and "Molecular Architectonics" 25110010), and Program for Key Interdisciplinary Research. S.I. thanks JSPS for financial support.

REFERENCES

(1) Qin, S.; Kim, J.; Niu, Q.; Shih, C. K. Superconductivity at The Two-Dimensional Limit. *Science* **2009**, *324*, 1314−1317.

DOI: 10.1021/acsnano.5b07848
ACS Nano XXXX, XXX, XXX−XXX

(2) Uchihashi, T.; Mishra, P.; Aono, M.; Nakayama, T. Macroscopic Superconducting Current Through A Silicon Surface Reconstruction with Indium Adatoms:Si(111)-($\sqrt{7}\times\sqrt{3}$)-In. *Phys. Rev. Lett.* **2011**, *107*, 207001.
(3) Yamada, M.; Hirahara, T.; Hasegawa, S. Magnetoresistance Measurements of A Superconducting Surface State of In-Induced and Pb-Induced Structures on Si(111). *Phys. Rev. Lett.* **2013**, *110*, 237001.
(4) Matetskiy, A. V.; Ichinokura, S.; Bondarenko, L. V.; Tupchaya, A. Y.; Gruznev, D. V.; Zotov, A. V.; Saranin, A. A.; Hobara, R.; Takayama, A.; Hasegawa, S. Two-Dimensional Superconductor with A Giant Rashba Effect: One-Atom-Layer Tl-Pb Compound on Si(111). *Phys. Rev. Lett.* **2015**, *115*, 147003.
(5) Ge, J. F.; Liu, Z. L.; Liu, C.; Gao, C. L.; Qian, D.; Xue, Q. K.; Liu, Y.; Jia, J. F. Superconductivity above 100 K in Single-Layer FeSe Films on Doped $SrTiO_3$. *Nat. Mater.* **2014**, *14*, 285−289.
(6) Xi, X.; Zhao, L.; Wang, Z.; Berger, H.; Forró, L.; Shan, J.; Mak, K. F. Strongly Enhanced Charge-Density-Wave Order in Monolayer $NbSe_2$. *Nat. Nanotechnol.* **2015**, *10*, 765−769.
(7) Ye, J. T.; Zhang, Y. J.; Akashi, R.; Bahramy, M. S.; Arita, R.; Iwasa, Y. Superconducting Dome in A Gate-Tuned Band Insulator. *Science* **2012**, *338*, 1193−1196.
(8) Novoselov, K. S.; Geim, A. K.; Morozov, S. V.; Jiang, D.; Katsnelson, M. I.; Grigorieva, I. V.; Dubonos, S. V.; Firsov, A. A. Two-Dimensional Gas of Massless Dirac Fermions in Graphene. *Nature* **2005**, *438*, 197.
(9) Novoselov, K. S.; Jiang, Z.; Zhang, Y.; Morozov, S. V.; Stormer, H. L.; Zeitler, U.; Maan, J. C.; Boebinger, G. S.; Kim, P.; Geim, A. K. Room-Temperature Quantum Hall Effect in Graphene. *Science* **2007**, *315*, 1379.
(10) Lee, C.; Wei, X.; Kysar, J. W.; Hone, J. Measurement of the Elastic Properties and Intrinsic Strength of Monolayer Graphene. *Science* **2008**, *321*, 385−388.
(11) Kim, K. S.; Zhao, Y.; Jang, H.; Lee, S. Y.; Kim, J. M.; Kim, K. S.; Ahn, J. H.; Kim, P.; Choi, J. Y.; Hong, B. H. Large-Scale Pattern Growth of Graphene Films for Stretchable Transparent Electrodes. *Nature* **2009**, *457*, 706−710.
(12) Bae, S.; Kim, H.; Lee, Y.; Xu, X.; Park, J. S.; Zheng, Y.; Balakrishnan, J.; Lei, T.; Kim, H. R.; Song, Y. I.; Kim, Y.-J.; Kim, K. S.; Özyilmaz, B.; Ahn, J. − H.; Hong, B. H.; Iijima, S. Roll-to-Roll Production of 30-Inch Graphene Films for Transparent Electrodes. *Nat. Nanotechnol.* **2010**, *5*, 574−578.
(13) Novoselov, K. S.; Geim, A. K.; Morozov, S. V.; Jiang, D.; Zhang, Y.; Dubonos, S. A.; Grigorieva, I. V.; Firsov, A. A. Electric Field Effect in Atomically Thin Carbon Films. *Science* **2004**, *306*, 666−669.
(14) Mazin, I. I.; Balatsky, A. V. Superconductivity in Ca-Intercalated Bilayer Graphene. *Philos. Mag. Lett.* **2010**, *90*, 731.
(15) Jishi, R. A.; Guzman, D. M.; Alyahyaei, H. M. Theoretical Investigation of Two-Dimensional Superconductivity in Intercalated Graphene Layers. *Adv. Studies Theor. Phys.* **2011**, *5*, 703.
(16) Ludbrook, B. M.; Levy, G.; Nigge, P.; Zonno, M.; Schneider, M.; Dvorak, D. J.; Veenstra, C. N.; Zhdanovich, S.; Wong, D.; Dosanjh, P.; Straßer, C.; Stöhr, A.; Forti, S.; Ast, C. R.; Starke, U.; Damascelli, A. Evidence for Superconductivity in Li-decorated Monolayer Graphene. *Proc. Natl. Acad. Sci. U. S. A.* **2015**, *112*, 11795−11799.
(17) Kanetani, K.; Sugawara, K.; Sato, T.; Shimizu, R.; Iwaya, K.; Hitosugi, T.; Takahashi, T. Ca Intercalated Bilayer Graphene as A Thinnest Limit of Superconducting C_6Ca. *Proc. Natl. Acad. Sci. U. S. A.* **2012**, *109*, 19610−19613.
(18) Xue, M.; Chen, G.; Yang, H.; Zhu, Y.; Wang, D.; He, J.; Cao, T. Superconductivity in Potassium-Doped Few-Layer Graphene. *J. Am. Chem. Soc.* **2012**, *134*, 6536−6539.
(19) Tiwari, A. P.; Shin, S.; Hwang, E.; Jung, S. G.; Park, T.; Lee, H. Superconductivity at 7.4 K in Few Layer Graphene by Li-intercalation. 2015, arXiv:physics/1508.06360. arXiv.org e-Print archive. http://arxiv.org/abs/1508.06360 (accessed Aug 27, 2015).
(20) Weller, T. E.; Ellerby, M.; Saxena, S. S.; Smith, R. P.; Skipper, N. T. Superconductivity in The Intercalated Graphite Compounds C_6Yb and C_6Ca. *Nat. Phys.* **2005**, *1*, 39−41.
(21) Emery, N.; Hérold, C.; d'Astuto, M.; Garcia, V.; Bellin, C.; Marêché, J. F.; Lagrange, P.; Loupias, G. Superconductivity of Bulk CaC_6. *Phys. Rev. Lett.* **2005**, *95*, 087003.
(22) Sugawara, K.; Sato, T.; Takahashi, T. Fermi-Surface-Dependent Superconducting Gap in C_6Ca. *Nat. Phys.* **2009**, *5*, 40−43.
(23) Yang, S. L.; Sobota, J. A.; Howard, C. A.; Pickard, C. J.; Hashimoto, M.; Lu, D. H.; Mo, S. − K.; Kirchmann, P. S.; Shen, Z. X. Superconducting Graphene Sheets in CaC_6 Enabled by Phonon-Mediated Interband Interactions. *Nat. Commun.* **2014**, *5*, 3493.
(24) Kyung, W.; Kim, Y.; Han, G.; Leem, C.; Kim, C.; Koh, Y.; Kim, B.; Kim, Y.; Kim, J. S.; Kim, K. S.; Rotenberg, E.; Denlinger, J. D.; Kim, C. Interlayer-State-Driven Superconductivity in CaC_6 Studied by Angle-Resolved Photoemission Spectroscopy. *Phys. Rev. B: Condens. Matter Mater. Phys.* **2015**, *92*, 224516.
(25) Li, K.; Feng, X.; Zhang, W.; Ou, Y.; Chen, L.; He, K.; Wang, L. L.; Guo, L.; Xue, Q. − X.; Ma, X. Superconductivity in Ca-Intercalated Epitaxial Graphene on Silicon Carbide. *Appl. Phys. Lett.* **2013**, *103*, 062601.
(26) Chapman, J.; Su, Y.; Howard, C. A.; Kundys, D.; Grigorenko, A.; Guinea, F.; Geim, A. K.; Grigorieva, I. V.; Nair, R. R. Superconductivity in Ca-doped Graphene. 2015, arXiv:physics/1508.06931. arXiv.org e-Print archive. http://arxiv.org/abs/1508.06931 (accessed Aug 27, 2015).
(27) Yamada, M.; Hirahara, T.; Hobara, R.; Hasegawa, S.; Mizuno, H.; Miyatake, Y.; Nagamura, T. Surface Electrical Conductivity Measurement System with Micro-Four-Point Probes at Sub-Kelvin Temperature under High Magnetic Field in Ultrahigh Vacuum. *e-J. Surf. Sci. Nanotechnol.* **2012**, *10*, 400−405.
(28) Sugawara, K.; Sato, T.; Kanetani, K.; Takahashi, T. Semiconductor−Metal Transition and Band-Gap Tuning in Quasi-Free-Standing Epitaxial Bilayer Graphene on SiC. *J. Phys. Soc. Jpn.* **2011**, *80*, 024705.
(29) Ohta, T.; Bostwick, A.; McChesney, J. L.; Seyller, T.; Horn, K.; Rotenberg, E. Interlayer Interaction and Electronic Screening in Multilayer Graphene Investigated with Angle-Resolved Photoemission Spectroscopy. *Phys. Rev. Lett.* **2007**, *98*, 206802.
(30) Lara-Avila, S.; Tzalenchuk, A.; Kubatkin, S.; Yakimova, R.; Janssen, T. J. B. M.; Cedergren, K.; Bergsten, T.; Fal'ko, V. Disordered Fermi Liquid in Epitaxial Graphene from Quantum Transport Measurements. *Phys. Rev. Lett.* **2011**, *107*, 166602.
(31) Kechedzhi, K.; Fal'ko, V. I.; McCann, E.; Altshuler, B. L. Influence of Trigonal Warping on Interference Effects in Bilayer Graphene. *Phys. Rev. Lett.* **2007**, *98*, 176806.
(32) Sugawara, K.; Kanetani, K.; Sato, T.; Takahashi, T. Fabrication of Li-Intercalated Bilayer Graphene. *AIP Adv.* **2011**, *1*, 022103.
(33) Larkin, A. I.; Aslamazov, L. G. The Influence of Fluctuation Pairing of Electrons on The Conductivity of Normal Metal. *Phys. Lett. A* **1968**, *26*, 238−239.
(34) Tinkham, M. *Introduction to Superconductivity*; Courier Corporation: New York, 2012; pp 110−143.
(35) Chaudhari, R. D.; Brown, J. B. Critical Currents in Superconducting Films of Indium. *Phys. Rev.* **1965**, *139*, A1482.
(36) Profeta, G.; Calandra, M.; Mauri, F. Phonon-Mediated Superconductivity in Graphene by Lithium Deposition. *Nat. Phys.* **2012**, *8*, 131−134.
(37) Calandra, M.; Attaccalite, C.; Profeta, G.; Mauri, F. Comment on "Electronic Structure of Superconducting KC_8 and Nonsuperconducting LiC_6 Graphite Intercalation Compounds: Evidence for a Graphene-Sheet-Driven Superconducting State". *Phys. Rev. Lett.* **2012**, *108*, 149701.

DOI: 10.1021/acsnano.5b07848
ACS Nano XXXX, XXX, XXX−XXX